

- Immunol.* **15**, 760 (1985); Y. Hashimoto, A. M. Maxam, M. I. Greene, *Proc. Natl. Acad. Sci. U.S.A.* **83**, 7865 (1986); L. E. Samelson, W. F. Davidson, H. C. Morse III, R. D. Klausner, *Nature* **324**, 674 (1986); L. D. Shultz and C. L. Sidman, *Annu. Rev. Immunol.* **5**, 367 (1987); S. Yokota *et al.*, *J. Immunol.* **139**, 2810 (1987).
54. R. C. Budd, M. Schreyer, G. C. Miescher, H. R. MacDonald, *J. Immunol.* **139**, 2200 (1987).
55. G. C. Miescher *et al.*, *ibid.* **138**, 1959 (1987).
56. W. F. Davidson, F. J. Dumont, H. G. Bedigian, B. J. Fowlkes, H. C. Morse, *ibid.* **136**, 4075 (1986).
57. K. Satyanarayana *et al.*, *Proc. Natl. Acad. Sci. U.S.A.* **85**, 8166 (1988).
58. F. Koning *et al.*, *Science* **236**, 834 (1987); W. A. Kuziel *et al.*, *Nature* **328**, 263 (1987).
59. G. Stingl *et al.*, *Proc. Natl. Acad. Sci. U.S.A.* **84**, 2430 (1987); G. Stingl *et al.*, *ibid.*, p. 4586.
60. V. Groh *et al.*, *J. Exp. Med.* **169**, 1277 (1989).
61. M. R. Rubenfeld *et al.*, *J. Invest. Dermatol.* **77**, 221 (1981); T. S. Kupper, D. L. Coleman, J. McGuire, D. Goldminz, M. C. Horowitz, *Proc. Natl. Acad. Sci. U.S.A.* **83**, 4451 (1986).
62. R. P. Bucy, C-L. H. Chen, J. Cihak, U. Losch, M. D. Cooper, *J. Immunol.* **141**, 2200 (1988); T. Goodman and L. Lefrancois, *Nature* **333**, 855 (1988); C. Janeway, *ibid.*, p. 804; M. Bonneville *et al.*, *ibid.* **336**, 479 (1989).
63. I am particularly grateful to B. Haynes, A. Kruisbeck, G. Miescher, and H. R. MacDonald for thoughtful and critical comments, and to M. Krangel and M. Brenner for initial help. Work in the author's laboratory has been supported by NIH research grants.

Research Articles

Three-Dimensional Spherical Models of Convection in the Earth's Mantle

DAVE BERCOVICI, GERALD SCHUBERT, GARY A. GLATZMAIER

Three-dimensional, spherical models of mantle convection in the earth reveal that upwelling cylindrical plumes and downwelling planar sheets are the primary features of mantle circulation. Thus, subduction zones and descending sheetlike slabs in the mantle are fundamental characteristics of thermal convection in a spherical shell and are not merely the consequences of the rigidity of the slabs, which are cooler than the surrounding mantle. Cylindrical mantle plumes that cause hotspots such as Hawaii are probably the only form of active upwelling and are therefore not just secondary convective currents separate from the large-scale mantle circulation. Active sheetlike upwellings that could be associated with mid-ocean ridges did not develop in the model simulations, a result that is in agreement with evidence suggesting that ridges are passive phenomena resulting from the tearing of surface plates by the pull of descending slabs.

OVER TIME SCALES OF MILLIONS OF YEARS AND LONGER, the earth's mantle behaves like a fluid. As the earth cools, the mantle fluid removes heat from the deep interior by the transport of mass, that is, by thermal convection. Mantle convection is generally accepted as the engine of plate tectonics (1) in that the rigid plates on the surface of the earth, whose relative motions create mountains, volcanoes, and earthquakes, are believed to be an integral part of the convective system and the surface expression of mantle convection. Accordingly, major plate tectonic features such

as the oceanic trenches or subduction zones (regions of convergence overlying cold downwelling currents), mid-ocean ridges (spreading regions delineating upwelling), and hotspots (areas with anomalously high volcanism and heat flow indicating upwelling) are thought to reveal something of the nature of the underlying mantle circulation.

Two-dimensional models of mantle circulation, although useful for exploring the vertical structure and heat flow characteristics of convection (1, 2), cannot be used to address some of the major features of tectonics and convection, namely the horizontal geometry of the trenches, ridges, and hotspots. Studies of three-dimensional convection in a plane layer have indicated that various horizontal convective patterns involving both upwelling and downwelling plumes and sheets are possible (3, 4). However, the thickness of the earth's mantle is nearly half the radius of the entire planet, suggesting that spherical geometry should be used to obtain representative results. Studies of three-dimensional convection in a spherical geometry have focused on a shell that is entirely heated at its base (5-7), even though the earth's mantle has a large amount of internal heating from the decay of radioactive isotopes and secular cooling (8). We have used numerical models to examine the combined effects of various heating modes and spherical geometry on the three-dimensional structure of convection. We find that several aspects of mantle convection and plate tectonics are basic features of three-dimensional convective flow in a spherical shell.

Numerical models. The numerical models solve the three-dimensional fluid dynamical equations of mass, momentum, and energy conservation in a spherical shell having a ratio of inner to outer radii typical of the earth's whole mantle (approximately 0.55). (We do not address the issue of whole-layer versus two-layer convection; rather, we assume that whole-mantle convection is occurring.) The top and bottom boundaries of the shell are assumed to be impermeable and free slip because the earth's surface (with mobile plates) and the core-mantle boundary (with an underlying liquid core) are essentially surfaces of zero shear stress. The mantle is

D. Bercovici and G. Schubert are in the Department of Earth and Space Sciences, University of California, Los Angeles, CA 90024. G. A. Glatzmaier is with the Earth and Space Sciences Division, Los Alamos National Laboratory, Los Alamos, NM 87545.

a highly viscous fluid (with a dynamic viscosity of approximately 10^{21} Pa·s), thus the effects of acceleration and the earth's rotation can be neglected. We have assumed that the mantle is compressible and that the density increases 60 percent from the top of the mantle to the bottom. Therefore, the effects of viscous dissipation and adiabatic heating from compression and expansion are included in the model. The effects of sound waves, which propagate many orders of magnitude faster than the fluid velocity, are removed with the anelastic approximation for the equation of mass conservation (6, 9). The bulk modulus (or adiabatic incompressibility) increases linearly with pressure in the model as prescribed by the Murnaghan equation (10); this increase corresponds approximately with bulk modulus variations in the earth's mantle. Thus, the pressure and density profiles for the hydrostatic, adiabatic rest state of the model are in good agreement with those derived from spherically symmetric seismic models of the earth (11). As is approximately true in the earth's mantle, the Grüneisen parameter (which relates adiabatic changes in temperature with changes in density) is assumed to be constant and equal to 1. Heat capacity is also assumed to be constant. Gravity is supplied by self-gravitation of the shell and a central gravity field from a homogeneous inner-lying core. This approach yields an acceleration of gravity in the model that is roughly constant in depth, in agreement with the seismically determined variations of gravity in the earth's mantle.

Other material parameters not prescribed by the equation of state for the adiabatic rest state are assumed to be constant. Thus, dynamic viscosity and thermal conductivity are constant throughout the shell. At the temperatures and pressures of the earth's interior, viscosity is dependent on pressure, temperature, and stress (thus, there is a nonlinear constitutive relation between stress and strain) (12). However, utilization of such a rheology in a three-dimensional model of convection is exceedingly complicated. As a first approximation, we employ a homogeneous Newtonian rheology and qualitatively discuss the possible effects of more realistic rheologies.

The earth's mantle is heated from below by the hotter underlying core and internally by both the decay of radionuclides (uranium, thorium, potassium) and secular cooling. Thermal history models (8) imply that the mantle is 70 to 80 percent internally heated. However, recent studies of the high-pressure melting temperature of iron (13) indicate that the temperature at the core-mantle boundary is considerably higher than was previously assumed and that a larger contribution of heat may come from the core. Given the uncertainty in the mode of heating the earth's mantle, we have made calculations for three different types of heating that cover the full range of

possible conditions in the mantle, from a shell entirely heated from below to one that is only internally heated. The internal heat generation supplies constant power output per unit mass.

The equations of motion and energy were solved with a spectral-transform method in space and a finite-difference method in time. In the spectral-transform method, both truncated series of orthonormal global functions (spherical harmonics for latitudinal and longitudinal dependence and Chebyshev polynomials for radial dependence) and a numerical grid were used to represent dependent variables (6, 9).

The spatial accuracy of a numerical solution depends on the energy spectrum of its spectral representation: a negligible amount of energy near the truncation (that is, smallest) wavelengths indicates that the truncation error is negligible and that the representa-

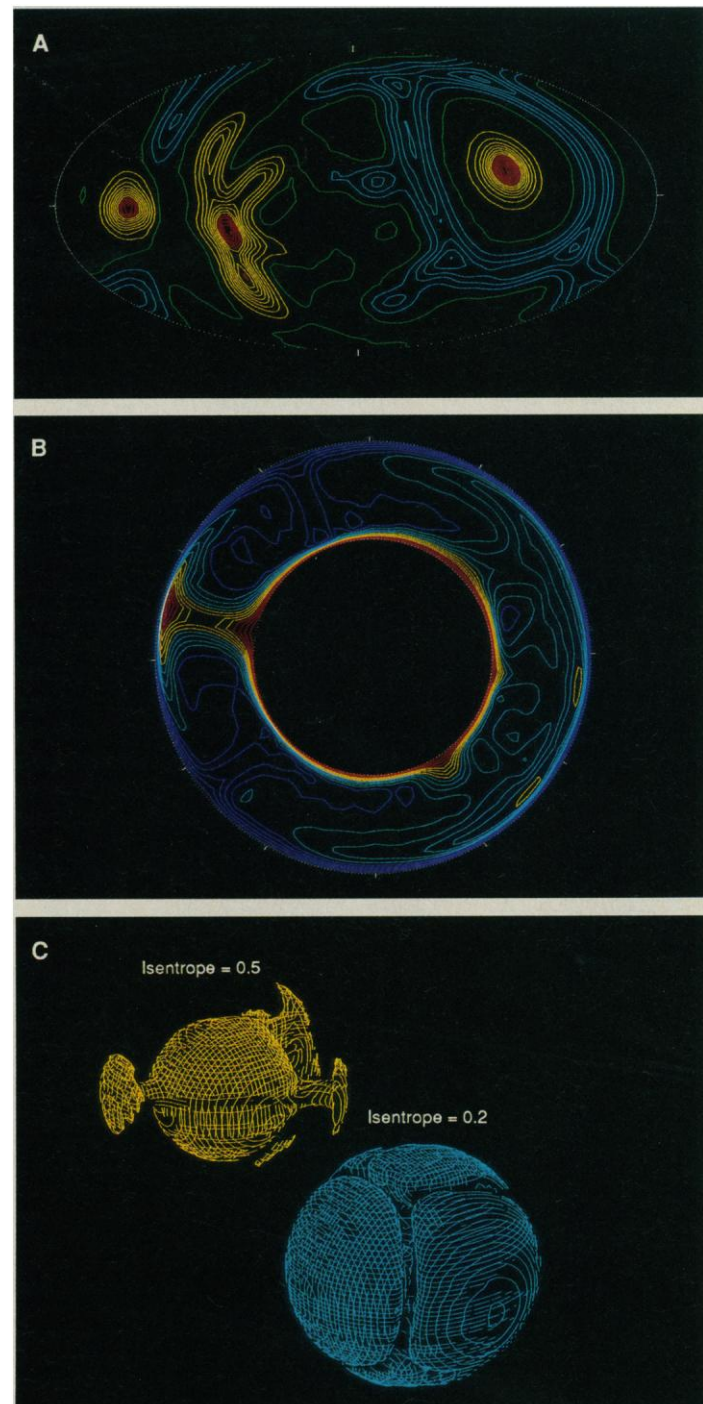


Fig. 1. Representative results for case A, in which the shell is entirely heated from below. **(A)** Contours of radial velocity w on a spherical surface midway through the spherical shell. The image is in an equal area projection. Colors represent equal intervals of velocity. Red contours are for w in the range $|w|_{\max} \geq w > |w|_{\max}/2$; yellow is for $|w|_{\max}/2 \geq w > 0$; green is for $w = 0$; light blue is for $0 \geq w > -|w|_{\max}/2$; blue is for $-|w|_{\max}/2 \geq w > -|w|_{\max}$. Dark blue colors do not appear on this frame because $|w|_{\max}$ occurs in the upwelling regions and the maximum downwelling velocity is $\leq |w|_{\max}/2$. Hence, downwelling is noticeably less vigorous than upwelling. **(B)** Contours of constant entropy in a cross section of the spherical shell along a plane of constant longitude. Entropy is used in compressible flow to show the advection of the thermal field by the convective currents (35). Red contours are for nondimensional values of entropy s in the "hot" range $1 \geq s > 3/4$, where $s = (S - S_{\min})/(S_{\max} - S_{\min})$, S is the dimensional value of entropy; yellow is for the "warm" range $3/4 \geq s > 1/2$; cyan is for the "cool" range $1/2 \geq s > 1/4$; blue is for the "cold" range $1/4 \geq s \geq 0$. **(C)** Three-dimensional surfaces of constant entropy. These surfaces are essentially single contours of constant entropy as in B extended out into three dimensions. The value of the isentrope shown on the figure corresponds to the nondimensional entropy s . The protrusions on the hotter (yellow) isentrope are cylindrical upwellings, whereas the canyons on the cold isentrope (blue) show the sheet-like downwellings.

tion is accurate. The energy spectra of the spherical harmonic series for the solutions in our model decrease by at least four orders of magnitude from the largest wavelength to the smallest (that is, the terms of the series near truncation have at most 0.01 percent of the largest spectral energy, which is usually contained in or near the first term of the series). The energy spectra of the Chebyshev series for the solutions decrease by at least five orders of magnitude from the

largest to the smallest wavelengths. Therefore, the numerical solutions are well resolved (14).

The accuracy and stability of the time integration are monitored by the Courant condition, which requires that the time step cannot exceed the minimum time needed for any fluid particle to travel between two points on the numerical grid. The numerical code has been tested successfully against another independently developed code; this comparison establishes that the numerical method is accurate (7).

Three cases are considered, all having the same adiabatic, static state. Calculations are initiated with random velocity, entropy, and pressure perturbations to this rest state (15). In case A, heating is entirely from below, and the boundaries are isothermal. In case B, heating is entirely internal, and the lower boundary is insulated while the upper boundary is isothermal. In case C, heating is both internal and from below, and the boundaries are isothermal. The proportion of heating that is from below is equal to the total heat entering the shell through its base divided by the total heat exiting the shell through its top. In case C, half of the heat comes from below.

The model calculations were carried out at a Rayleigh number $Ra \approx 100Ra_{cr}$, where Ra is a nondimensional measure of convective vigor and Ra_{cr} is the critical Rayleigh number for the onset of convection. This Ra is approximately one order of magnitude below the range of Rayleigh numbers for the earth's whole mantle (1). The convective vigor of the earth's mantle is not satisfactorily resolvable with our numerical models because of present-day limitations on computer memory. Higher Rayleigh numbers may lead to quantitative differences in the solutions. However, laboratory experiments with three-dimensional plane-layer convection (4) show that the qualitative nature of the convective patterns (that is, the structure and geometry of upwelling and downwelling regions)—and even the convective patterns themselves—do not change significantly as the Rayleigh number increases from $\sim 100Ra_{cr}$ to $\sim 400Ra_{cr}$ (16). Moreover, in earlier work with this numerical code for purely basally heated convection (6), solutions for $Ra \approx 1000Ra_{cr}$ (although less spatially resolved than those with $Ra \approx 100Ra_{cr}$) have convective patterns similar to those in case A. Therefore, we expect that the qualitative forms of convection that characterize our solutions are relevant to the style of convection in the earth's mantle.

Three-dimensional structure of convection. In all of the simulations that we have made for case A, in which the shell is entirely heated from below, the convective pattern is dominated by large cylindrical upwelling plumes surrounded by a network of downwelling sheets (Fig. 1, A and C); this pattern is characteristic of convection for a spherical shell heated from below (7). The maximum velocity in the upwelling regions was always greater than that in the regions of downwelling. Even though the whole convective pattern drifts and the number of upwelling plumes diminishes with time (through fusion of plumes at their bases), the sheetlike downwellings and cylindrical upwellings steadily persisted throughout all calculations. The thicknesses of the downwelling sheets were typically 1000 km. The thicknesses of upwelling and downwelling currents, which are determined by the thicknesses of the thermal boundary layers, will be smaller for the larger Rayleigh numbers that are more representative of the real mantle.

The upwelling plumes emanated from the thermal boundary layer at the base of the shell and maintained a concentrated thermal anomaly while traversing the shell (Fig. 1B). In contrast, the thermal gradients across the downwelling sheets were not as large as across the upwelling regions. The difference in the thermal anomalies and velocities of the upwelling and downwelling regions is a result of the inherent spherical geometry in that the bottom boundary of the shell has less surface area than the top boundary. Because the net heat

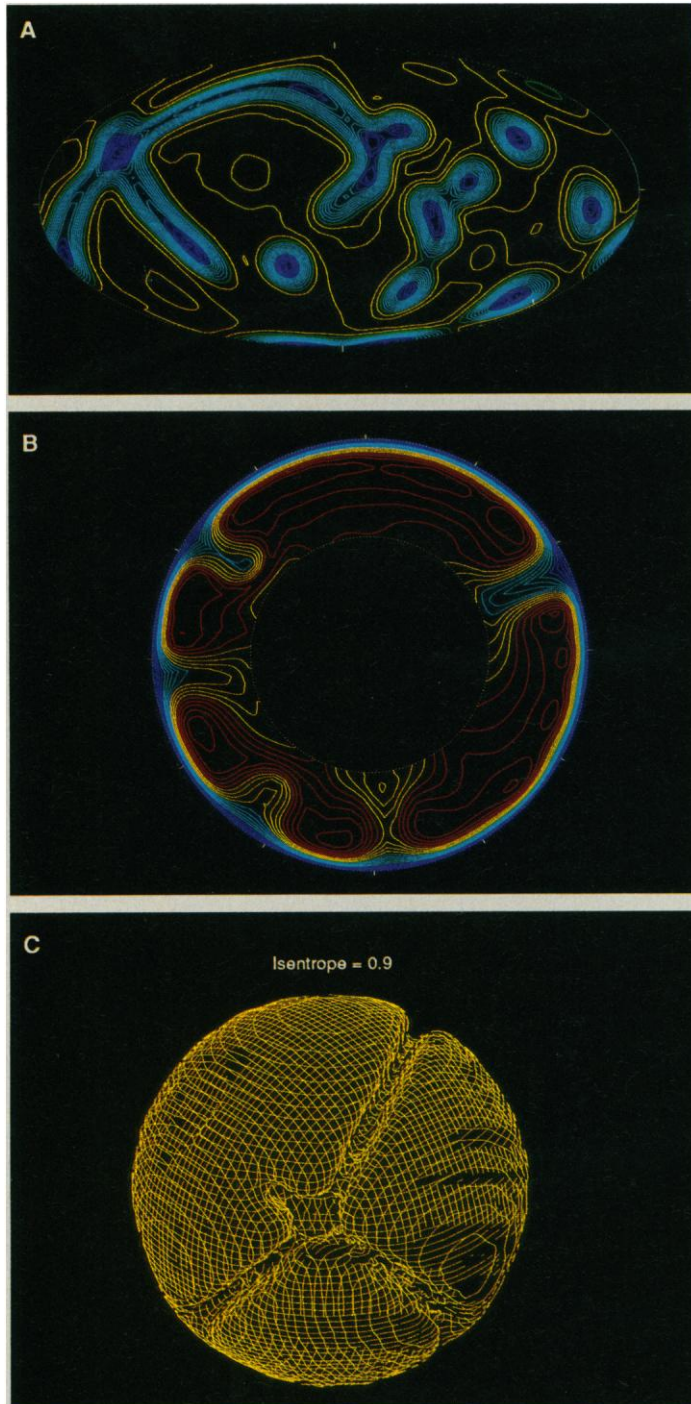


Fig. 2. Representative results for case B, in which the spherical shell is entirely internally heated. (A) Contours of radial velocity, as described in Fig. 1. Red contours do not appear in this frame because the maximum downwelling velocity is at least twice as fast as the maximum upwelling velocity. (B) Contours of constant entropy, as described in Fig. 1. (C) Three-dimensional surface of constant entropy. Because upwelling is present as a weak background flow, even the hot isentropes shown displays only the long linear canyons that delineate the downwelling sheets.

flow (which is proportional to surface area) into the shell must on average equal the net heat flow out of the shell, and because the upper and lower boundary layers are of comparable thickness, the temperature drop across the bottom thermal boundary layer is greater than the temperature drop across the upper one. Thus, fluid rising from the base of the shell has a greater thermal anomaly and hence a larger buoyancy anomaly than the fluid sinking from the top of the shell.

In the simulations of case B, in which the shell is entirely heated from within, the horizontal convective pattern has both cylindrical and long sheetlike downwellings and broad regions of weak upwelling (Fig. 2, A and C). The cylindrical downwellings were transient, whereas the downwelling sheets had great horizontal extent and were long-lived, usually persisting for the entire simulation. The downwelling sheets in case B were also segmented instead of interconnected as in case A. The presence of durable downwelling sheets in the basally heated models occurs because the sheets are the return flow to the cylindrical upwellings and must therefore form a cylindrical wall around the plumes. The formation of persistent descending sheets in the case of internally heated convection was unexpected. Because the sheets do not form in response to any upwelling plumes, they are essentially self-organizing structures.

In contrast to case A, the largest velocities and thermal anomalies in case B occurred in the downwelling regions rather than in the upwelling regions (Fig. 2, A and B). This difference occurs because there is no thermal boundary layer along the base of the shell in case B (as it is insulated), thus the largest thermal and buoyancy anomalies occur in the upper boundary layer.

In the simulations of case C, in which the shell is half internally and half basally heated, the convective pattern closely resembled that of case A; upwelling occurred as cylindrical plumes embedded in a network of downwelling sheets (Fig. 3, A and C). However, the downwelling regions were more intense (that is, they had larger velocities and thermal anomalies) than in case A (Fig. 3, A and B). The boundary layers at the top and bottom of the shell with both internal and basal heating had comparable temperature drops; thus, the thermal and buoyancy anomalies of the upwelling and downwelling regions were of approximately equal magnitude.

More upwelling plumes were present in case C than in case A, possibly because the stronger downwelling in case C inhibited the coalescence of upwelling plumes. Case C appears to infuse the intensity of the downwelling sheets from case B into the downwelling pattern characteristic of case A.

Implications for mantle dynamics. Although the model calculations lack much of the complexity of the earth's mantle (for example, rheological dependences and discontinuities from phase or compositional changes), several features of the simulations show significant similarities with various aspects of convection in the earth's mantle. The most striking feature of all three calculations is that, even though the patterns and nature of convection vary with changes in heating mode, the dominant style of downwelling is consistently in the form of long, linear sheets or slabs. Descending slabs in the earth's mantle have usually been thought to occur because the lithospheric plates that become unstable and sink are rigid: the temperature dependence of mantle-silicate rheology and the relatively cooler temperature of the lithosphere with respect to the mantle would allow the slabs to maintain their planar structure as they penetrate into the mantle. However, the results of this work show that downwelling slabs or sheets are a natural occurrence of the dynamics of three-dimensional convective flow in a spherical geometry, even for a simple Newtonian rheology.

The addition of temperature-dependent rheology is certainly important in enhancing the survivability of the downwelling sheets by increasing their viscosity many orders of magnitude (17). Whether

a temperature-dependent rheology is solely responsible for maintaining the planar structure of subducting plates by keeping them rigid is another question. Viscosity increases with depth due to phase or compositional changes, or from the dependence of rheology on pressure, tend to offset the effect of the temperature dependence by reducing the viscosity contrast between the mantle and the slab. An actual subducting slab may also be too thin (roughly 100

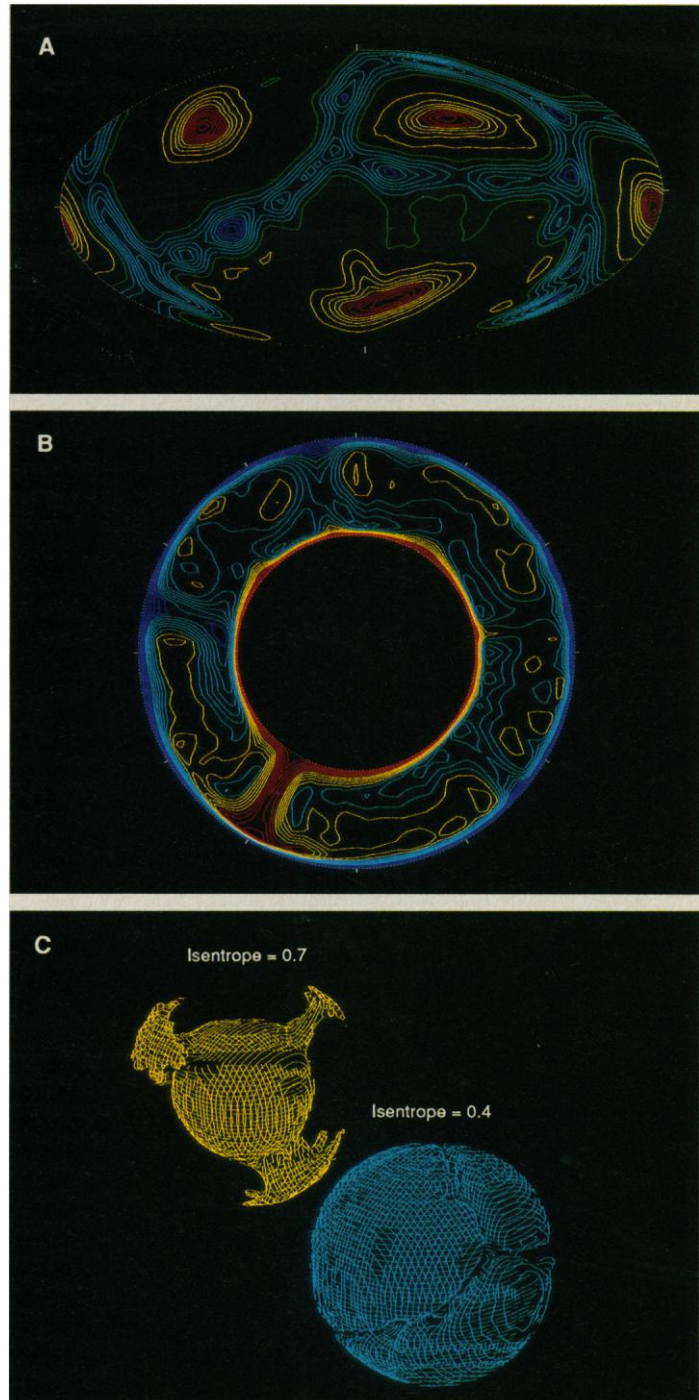


Fig. 3. Representative results for case C, in which the spherical shell is half heated from below and half internally heated. (A) Contours of radial velocity, as described in Fig. 1. All colors appear in this frame because the upwelling and downwelling velocities are comparable. (B) Contours of constant entropy, as described in Fig. 1. (C) Three-dimensional surfaces of constant entropy. Surfaces with similar shape to those in Fig. 1 are visible at warmer isentropes because the mean entropy is higher as a result of the internal heating.

km compared to a 40,000-km global circumference) to resist a mantle flow that might act to deform it into something other than a sheet. Finally, a rheology that is only dependent on temperature may actually prevent the formation of descending slabs since it leads to a rigid, stagnant lid at the upper thermal boundary layer which is decoupled from the rest of the flow (17, 18); this is less like the earth than the constant viscosity case. Subducting slabs probably occur because other rheological effects, such as strain-softening and lubrication by water and sediment (19), counteract the influence of temperature-dependent viscosity.

Although the importance of variable viscosity cannot be disregarded, our calculations show that sheetlike downwellings occur for a simple rheology and for any heating mode. Thus, one of the most salient features of plate tectonics—subducting, descending slabs—is a robust and fundamental property of the basic fluid dynamics of three-dimensional convection in a spherical shell. These results suggest that oceanic trenches and the descending lithospheric plates they delineate are an integral part of global mantle circulation.

The model results also show that with basal heating, upwelling is in the form of cylindrical plumes. Mantle plumes and their surface expressions as hotspots have traditionally been thought to reflect the effects of temperature-dependent rheology, arising as secondary instabilities in the hot, low viscosity thermal boundary layer at the base of the mantle (20). They are also perceived to be essentially decoupled from the large-scale flow that drives the plates and hence are reference points against which plate motions may be measured (21). The simulations of this study suggest that cylindrical mantle plumes, rather than a secondary instability, are the only form of upwelling from the base of the mantle. However, a temperature-dependent rheology is important in accounting for the narrowing of mantle plumes and thinning of the lithosphere at intraplate hotspots. These results also imply that the active upwelling portion of mantle convection is at least a whole-layer phenomenon.

In contrast, upwelling sheets that might be associated with mid-ocean ridges do not occur in any of the cases that have some component of heating from below. In addition, hotspots do not in general coincide with mid-ocean ridges. The model results thus indicate that mid-ocean ridges are not a consequence of active upwelling from the deep mantle. This interpretation is in agreement with the hypothesis that the upwelling beneath ridges is a shallow and passive response to the tearing of tectonic plates under the pull of sinking slabs (22). Concentrated linear regions of shallow upwelling and extension do not appear in our models because they probably require a rigid lithosphere to act as a stress guide for the tension supplied by the slabs, and a brittle-fracture or plastic rheology to give sharp or discontinuous features of extensional strain. Hotspots that do occur along mid-ocean ridges (for example, Iceland) either may have catalyzed the initial weakening of the lithosphere leading to a rift, or were possibly drawn to the spreading regions because the thinner lithosphere facilitated the heat transport of the plumes.

This picture of thermal convection in the mantle, as indicated by the numerical solutions, is supported by various geophysical observations. Considerable evidence suggests that after the cold, dense lithosphere subducts, the resultant descending slab becomes an integral part of circulation throughout the mantle. Benioff zones are regions of high seismicity that delineate sinking slabs to a depth of approximately 670 km (23, 24). The focal mechanisms of earthquakes near the bases of Benioff zones are characteristic of compressional deformation, implying that the 670-km discontinuity (a sharp transition region in seismic velocity attributed either to a phase or to a compositional change) hinders further slab penetration (24, 25). However, recent analyses of seismic travel-time anomalies (wherein a seismically fast, and presumably cold, heterogeneity such as a slab

is identified because travel times for waves that traverse the slab along its plane are shorter than those for waves that travel perpendicular to its plane) provide evidence of slab penetration into the deep mantle (26). Seismic tomography has shown that a ring of seismically fast and presumably cold material occurs beneath subduction zones around the Pacific and extends into the deep lower mantle (27); both gravity and seismic analyses have shown that there is an associated depression of the core-mantle boundary (28, 29). These data imply that the descending slabs are at least felt at the base of the mantle even if they do not reach the core-mantle boundary (30). The ringlike geometry of the Pacific downwelling closely resembles the configuration of downwelling sheets in all three model calculations.

Both seismic and gravity data support the concept of mantle upwelling indicated by the models with some component of basal heating. The relation of long wavelength geoid anomalies and seismically slow mantle heterogeneity with the worldwide distribution of hotspots suggests that mantle plumes are active upwellings from the lower mantle (29–31) and are, therefore, part of the mantlewide circulation. Alternatively, seismic tomography shows that seismically slow and presumably hot regions beneath mid-ocean ridges do not extend deeper than about 350 km into the mantle (32); these data are consistent with our models and suggest that the upwelling beneath ridges has a shallow origin. In addition, ridges have a negligible geoid signature (29–31), which suggests that they are isostatically compensated. Because active upwelling would necessarily create dynamically supported topography, and hence a considerable geoid signature, the ridges are not the result of active upwelling (22).

The geophysical evidence that the upwelling beneath ridges is passive has led some investigators to argue that most, if not all, of the heating of the mantle is internal (33). Our results suggest that the ridges are passive not because the mantle is only heated from within but because the active upwelling characteristic of basal heating is occurring elsewhere, at the mantle plumes.

Our model calculations are successful at accounting for the geometry of the upwelling and downwelling currents of mantle convection, and therefore the morphology of the divergent and convergent features of plate tectonics. However, without further rheological complexity, these models cannot address the occurrence of the tectonic plates themselves or the motion along transform faults. Both phenomena could probably result from a laterally heterogeneous viscosity in the mantle (which results from the dependence of silicate rheology on temperature, pressure, and stress) or nonviscous behavior in the lithosphere (for example, brittle fracture and plasticity) (34). The study of three-dimensional spherical convection with more realistic rheologies is the next major step in the dynamic modeling of the earth's mantle.

REFERENCES AND NOTES

1. E. R. Oxburgh and D. L. Turcotte, *Rep. Prog. Phys.* **41**, 1249 (1978); G. Schubert, *Annu. Rev. Earth Planet. Sci.* **7**, 289 (1979); D. L. Turcotte and G. Schubert, *Geodynamics* (Wiley, New York, 1982).
2. There is an extensive body of literature on numerical models of two-dimensional plane layer convection, for example, G. Schubert and C. Anderson, *Geophys. J. R. Astron. Soc.* **80**, 575 (1985), and references therein; A. T. Hsui, D. L. Turcotte, K. E. Torrance, *Geophys. Fluid Dyn.* **3**, 35 (1972); G. Schubert and A. Zebib, *Geophys. Astrophys. Fluid Dyn.* **15**, 65 (1980); A. Zebib, G. Schubert, J. M. Strauss, *J. Fluid Mech.* **97**, 257 (1980); A. Zebib, G. Schubert, J. L. Dein, R. C. Paliwal, *Geophys. Astrophys. Fluid Dyn.* **23**, 1 (1983); A. Zebib, A. K. Goyal, G. Schubert, *J. Fluid Mech.* **152**, 39 (1985); P. Machetel and M. Rabinowicz, *Geophys. Res. Lett.* **12**, 227 (1985); P. Machetel and D. A. Yuen, *ibid.* **13**, 1470 (1986); *Earth Planet. Sci. Lett.* **86**, 93 (1987); D. Bercovici, G. Schubert, A. Zebib, *J. Geophys. Res.* **93**, 6430 (1988).
3. F. H. Busse, *Rep. Prog. Phys.* **41**, 1929 (1978); B. Travis, P. Olson, G. Schubert, *J. Fluid Mech.*, in press.
4. J. A. Whitehead and B. Parsons, *Geophys. Astrophys. Fluid Dyn.* **9**, 201 (1978).
5. R. E. Young, *J. Fluid Mech.* **63**, 695 (1974); F. H. Busse, *ibid.* **72**, 67 (1975); F.

- H. Busse and N. Riahi, *ibid.* **123**, 283 (1982); P. Macheret, M. Rabinowicz, P. Bernadet, *Geophys. Astrophys. Fluid Dyn.* **37**, 57 (1986).
6. G. A. Glatzmaier, *Geophys. Astrophys. Fluid Dyn.* **43**, 223 (1988).
 7. D. Bercovici, G. Schubert, G. A. Glatzmaier, A. Zebib, *J. Fluid Mech.*, in press.
 8. G. Schubert, D. Stevenson, P. Cassen, *J. Geophys. Res.* **85**, 2531 (1980); G. F. Davies, *ibid.*, p. 2517 (1980).
 9. G. A. Glatzmaier, *J. Comp. Phys.* **55**, 461 (1984).
 10. F. D. Murnaghan, *Finite Deformation of an Elastic Solid* (Wiley, New York, 1951).
 11. A. M. Dziewonski and D. L. Anderson, *Phys. Earth Planet. Inter.* **25**, 297 (1981).
 12. J. Weertman and J. R. Weertman, *Annu. Rev. Earth Planet. Sci.* **3**, 293 (1975).
 13. Q. Williams, R. Jeanloz, J. Bass, B. Svendsen, T. J. Ahrens, *Science* **236**, 181 (1987).
 14. The truncation of the spherical harmonic series was at spherical harmonic degree and order 32. The truncation of the Chebyshev series was at order 20 for cases A and C, and order 16 for case B. The physical space grid had 96 longitudinal points and 48 latitudinal points, and either 41 (cases A and C) or 33 (case B) Chebyshev radial collocation points. The grid spacing was, therefore, 3.8° in either horizontal direction. The radial grid spacing was either 4 km (cases A and C) or 7 km (case B) near the boundaries, and either 115 km (cases A and C) or 140 km (case B) near the middle of the shell. (Chebyshev collocation points are densely spaced near the boundaries of the domain of the Chebyshev polynomials; this allows for greater resolution in the boundary layers.) The shell thickness is 2885 km.
 15. The model calculations were carried out for a variety of initial conditions. Although the solutions may differ quantitatively for different initial conditions, the basic structure of the upwelling and downwelling regions remains constant for a given heating mode. In these models of compressible spherical convection, there are, in addition to the Rayleigh number, the Gr \ddot{u} neisen parameter and the ratio of the inner radius to the outer radius, six nondimensional parameters. Four of these parameters are the same for all three cases; they are the dissipation number $Di = \ln(T_{bot}/T_{top}) = 0.5$ (where T_{bot} and T_{top} are the bottom and top temperatures of the adiabatic reference state), $4\pi G \rho_{bot} d/g_{bot} = 1.26$ (where G is the gravitational constant, ρ_{bot} is the bottom density of the adiabatic reference state, d is the shell thickness, and g_{bot} is the gravity at the bottom of the shell due to the core), $c_p T_{bot}/g_{bot} d = 0.12$ (where c_p is the heat capacity at constant pressure), and $K' = 3.5$ (where K' is the slope of the linear relation of bulk modulus as a function of pressure prescribed by the Murnaghan equation). The two remaining parameters are dependent on the relative amounts of internal and basal heating; they are, for cases A, B and C, respectively, $(\Delta T_{sa} + \rho_{bot} \epsilon d^2/k)/T_{bot} = 1, 13.9,$ and 2.4 (where ΔT_{sa} is the superadiabatic temperature drop across the shell and represents the amount of basal heating, ϵ is the rate of internal heat generation in units of power per unit mass, and k is thermal conductivity), and $\Delta T_{sa}/(\Delta T_{sa} + \rho_{bot} \epsilon d^2/k) = 1, 0,$ and 0.14 . Study of the effects of variations in these parameters suggests that so long as the amount of heat input into the shell is much larger than the heat that can be carried conductively along the adiabatic temperature gradient (as in these models), the calculations are relatively insensitive to these additional parameters. All model calculations were time-integrated through approximately ten runs, with 1000 time steps per run. The time step was between 1 million years and 10 million years (because the time step size is determined by the fluid velocities which are different from one case to another), hence a complete simulation represented a 10- to 100-billion-year time lapse. These times are not physically significant in that the convective vigor of the simulations was less than that of the earth's mantle. When a simulation was started, convection began immediately and the convective pattern was fully developed within the first 1000 time steps.
 16. The laboratory experiments of (4) were performed for $Ra \leq 760,000$ for rigid top and bottom boundaries. The Ra_{cr} for a plane layer of infinite horizontal extent with rigid isothermal top and bottom boundaries is 1708. However, because the experimental apparatus had rigid side walls, and the upper and lower boundaries were not perfectly isothermal, the actual Ra_{cr} may have been different from the theoretical value.
 17. U. R. Christensen and D. A. Yuen, *J. Geophys. Res.* **89**, 4389 (1984); M. Gurnis and B. H. Hager, *Nature* **335**, 317 (1988).
 18. D. White, *J. Fluid Mech.* **191**, 247 (1988).
 19. P. Bird, *Geophys. J. R. Astron. Soc.* **55**, 411 (1978); R. L. Shreve and M. Cloos, *J. Geophys. Res.* **91**, 10229 (1986).
 20. D. A. Yuen and G. Schubert, *J. Geophys. Res.* **81**, 2499 (1976); D. E. Loper and F. D. Stacey, *Phys. Earth Planet. Inter.* **33**, 304 (1983); P. Olson, G. Schubert, C. Anderson, *Nature* **327**, 409 (1987); P. Olson, G. Schubert, C. Anderson, P. Goldman, *J. Geophys. Res.* **93**, 15065 (1988).
 21. W. J. Morgan, *Nature* **230**, 42 (1971); *Am. Assoc. Petrol. Geol. Bull.* **56**, 203 (1972); *The Sea*, vol. 7, C. Emiliani, Ed. (Wiley-Interscience, New York, 1981).
 22. A. H. Lachenbruch, *J. Geophys. Res.* **81**, 1883 (1976).
 23. H. Benioff, *Bull. Geol. Soc. Am.* **60**, 1837 (1949); B. Isacks, J. Oliver, L. R. Sykes, *J. Geophys. Res.* **73**, 5855 (1968).
 24. B. Isacks and P. Molnar, *Rev. Geophys. Space Phys.* **9**, 103 (1971).
 25. F. M. Richter, *J. Geophys. Res.* **84**, 6783 (1979); D. Giardini and J. H. Woodhouse, *Nature* **307**, 505 (1984).
 26. T. H. Jordan, *J. Geophys. Res.* **43**, 473 (1977); K. C. Creager and T. H. Jordan, *J. Geophys. Res.* **89**, 3031 (1984); *ibid.* **91**, 3573 (1986); K. M. Fischer, T. H. Jordan, K. C. Creager, *ibid.* **93**, 4773 (1988).
 27. A. M. Dziewonski, *J. Geophys. Res.* **89**, 5929 (1983); A. M. Dziewonski and J. H. Woodhouse, *Science* **236**, 37 (1987).
 28. A. Morelli and A. M. Dziewonski, *Nature* **325**, 678 (1987).
 29. B. H. Hager, R. W. Clayton, M. A. Richards, R. P. Comer, A. M. Dziewonski, *ibid.* **313**, 541 (1985).
 30. P. G. Silver, R. W. Carlson, P. Olson, *Annu. Rev. Earth Planet. Sci.* **16**, 477 (1988).
 31. C. G. Chase, *Nature* **282**, 464 (1979); S. T. Crough and D. M. Jurdy, *Earth Planet. Sci. Lett.* **48**, 15 (1980); M. A. Richards, B. H. Hager, N. H. Sleep, *J. Geophys. Res.* **93**, 7690 (1988).
 32. J. H. Woodhouse and A. M. Dziewonski, *J. Geophys. Res.* **89**, 5953 (1984).
 33. G. F. Davies, *ibid.*, p. 10467 (1988).
 34. W. M. Kaula, *ibid.* **85**, 7031 (1980); B. H. Hager and R. J. O'Connell, *ibid.* **86**, 4843 (1981); A. M. Forte and W. R. Peltier, *ibid.* **92**, 3645 (1987); M. Gurnis, *Nature* **332**, 695 (1988).
 35. Entropy is a measure of the heat content of the fluid, and, if convection is vigorous, the fluid will transport its heat with little loss from diffusion. Convecting fluid thus moves essentially adiabatically, that is, with constant entropy. Therefore, contours of constant entropy trace the advection of heat. Entropy is also closely related to potential temperature, which is often used in atmospheric and oceanographic sciences as a measure of temperature corrected for the effects of pressure, such as compressional heating. In incompressible flow, entropy, like potential temperature, is interchangeable with absolute temperature.
 36. We thank R. J. Willemann and D. V. Kemp for useful discussions regarding subduction zones and descending slabs, as well as an anonymous reviewer for helpful comments. This work has benefited from the mantle convection workshop sponsored by the Institute of Geophysics and Planetary Physics at the Los Alamos National Laboratory. It was supported by a grant from the National Aeronautics and Space Administration (NAG 5152) and a computing grant from the San Diego Supercomputer Center. Computing and graphics were done on a Cray XMP-48 and a DICOMED D48CR film recorder at the San Diego Supercomputer Center.

23 January 1989; accepted 18 April 1989

1989 AAAS Philip Hauge Abelson Prize To Be Awarded to a Public Servant or Scientist

The AAAS Philip Hauge Abelson Prize of \$2,500 and a commemorative plaque, established by the AAAS Board of Directors in 1985, is awarded annually either to:

- (a) a public servant, in recognition of sustained exceptional contributions to advancing science, or
- (b) a scientist whose career has been distinguished both for scientific achievement and for other notable services to the scientific community.

AAAS members are invited to submit nominations now for the 1989 prize, to be awarded at the 1990 Annual Meeting in New Orleans. Each nomination must be seconded by at least two other AAAS members. The prize recipient will be

selected by a seven-member panel appointed by the Board. The recipient's travel and hotel expenses incurred in attending the award presentation will be reimbursed.

Nominations should be typed and should include the following information: nominee's name, institutional affiliation and title, address, and brief biographical resume; statement of justification for nomination; and names, identification, and signatures of the three or more AAAS member sponsors.

Eight copies of the complete nomination should be submitted to the AAAS Office of Public Sector Programs, 1333 H Street, N.W., Washington, D.C. 20005, for receipt on or before 1 August 1989.